Seasonal types in homogeneous rainfall regions of the Amazon basin

Véronique Michot, Thomas Corpetti, Josyane Ronchail, Jhan Carlo Espinoza, Damien Arvor, Beatriz M Funatsu, Vincent Dubreuil

Seasonal types in homogeneous rainfall regions of the Amazon basin

Véronique Michot[1], Thomas Corpetti[2], Josyane Ronchail[3], Jhan Carlo Espinoza[4], Damien Arvor[2], Beatriz M. Funatsu[5], Vincent Dubreuil[2]

[1]Université Paris Cité, UMR 8586 PRODIG, 75013 Paris, France, veronique.michot@u-paris.fr
[2]UMR 6554 LETG, Université Rennes 2, CNRS, 35000 Rennes, France, thomas.corpetti@univ-rennes2.fr, vincent.dubreuil@univ-rennes2.fr , damien.arvor@univ-rennes2.fr
[3]Laboratoire d'Océanographie et du Climat, LOCEAN-IPSL, Sorbonne Université, IRD, CNRS, MNHN, Paris, France, josyane.ronchail@locean.ipsl.fr
[4]Université Grenoble Alpes, IRD, CNRS, Grenoble INP, Institut des Géosciences de l'Environnement (IGE, UMR 5001), Grenoble, France. Universidad Católica del Perú (PUCP). Lima, Peru, jhan-carlo.espinoza@ird.fr
[5]CNRS, LETG UMR6554, Nantes Université, Campus Tertre Bâtiment IGARUN, 44312 Nantes cedex 3, beatriz.funatsu@univ-nantes.fr

Abstract

Due to its size and geographical features, different average annual rainfall regimes co-exist in the Amazon basin, with distinct year-to-year variability dependent on regions within the basin. In this study, we define and explain the seasonal regional types of annual regimes, i.e., years with similar seasonal anomalies. Our work is based on a 205 rain gauge network distributed over 5 Amazonian countries, spanning a period over 30 years. Using a spectral clustering method, we identified 7 sub-regions within the basin in which annual rainfall regimes are spatially homogenous. For each sub-domain we estimate specific parameters that characterize the rainy season (onset and demise dates, sign and duration of rainfall anomalies). Finally, using spectral analysis we identify between 2 and 4 "seasonal type" of precipitation in these seven sub-domains. Most of these seasonal types are in phase with the large-scale atmospheric circulation, which explain the temporal link with rainfall anomalies. The seasonal types result of the superposition of interannual and intra-seasonal variability whose factors are then difficult to identify and attribute. Part of the rainfall anomalies characterizing seasonal types is related to the interannual variability of the sea surface temperature in the Atlantic or the Pacific oceans, especially in the North-East and South-East part of the Amazon Basin, while in other parts strong intra-seasonal and local factors have a larger impact. The same sign and duration of anomalies do not concomitantly affect the various regions of the Amazon Basin, confirming that one mode of variability does not homogeneously affect precipitation in different parts of the basin.

Key words: precipitation regimes, seasonal type, rain gauge network, spectral clustering, sea surface temperature

I. INTRODUCTION

The Amazon basin (AB) is very often reduced to the mere image of evergreen forest continuously showered with large amounts of rain. However, the diversity of environments and precipitation regimes are complex and stems in particular from the size of the Amazonian watershed, which extends from the Andes to the Atlantic covering more than six million km². Located in the intertropical zone between 5°N and 20°S, the AB regional climate is regulated by the South American monsoon, the displacement of the Intertropical convergence zone (ITCZ), and on their seasonality (Vera *et al.*, 2006). Average precipitation and rainfall regimes are highly contrasted (see, e.g., Figueroa and Nobre, 1990; Marengo, 1992; Espinoza Villar *et al.*, 2009 ; among others). According to the Köppen climate classification, the basin falls within a type A warm climate, with subtypes Af (tropical wet without a dry season) in the west and along the Negro River, and Am (tropical monsoon) and Aw (tropical savanna with dry winter) in the north, northeast, south and southeast. In the equatorial Amazon-Andes transition zone, several

seasonal rainfall regimes are identified in few kilometers due to the interaction between regional atmospheric circulation and the Andean topography (Laraque *et al.*, 2007; Espinoza *et al.*, 2009; Segura *et al.*, 2019). Between 50 and 70% of rainfall in the Amazon basin comes from the Atlantic via moisture advection, variable according to the season, through the ITCZ (Costa and Foley 1999; Durieux 2002; Wang and Fu 2002; Arraut and Satyamurty 2009; 2012; Satyamurty et al. 2013). Moisture flows enter the basin mainly to the east at around 45°W and to the north. Convective systems are able to reach the Andes thanks to contribution of synoptic circulation and evapotranspiration from the Amazon rainforest (Simões Reibota et al. 2010 ; Segura et al., 2020). The Amazon rainforest feeds the atmosphere with moisture through evapotranspiration, and it is estimated that between 33% and 56% of precipitation comes from evapotranspiration (Molion 1975; Marques et al. 1977; Salati et al. 1978; Makarieva et al. 2007; Satyamurty et al. 2013; Rocha et al. 2015). However, southern and south-western Amazonia differ, with a greater contribution from local recycling by vegetation in the former region than in the latter, which in turn depends on evapotranspiration in other parts of the basin (Staal et al., 2018). Some of the moisture in the Amazon basin is also transported southwards towards the subtropical regions of southern South America via the Low Level Jet east of the Andes (Salio et al. 2002; Arraut and Satyamurty 2009) and then is also a source of moisture for the Plata basin. The seasonal precipitation regimes in the Amazon basin are however highly variable from one year to another when compared to the historical mean seasonal regime. Therefore, a high variability in the different parameters of the rainy season can be observed, for instance in its duration and the onset and demise of the rainiest period, the occurrence of dry spells, or in the intensity of intra-seasonal rainfall (e.g., (Moron, Camberlin and Robertson, 2013; Arvor *et al.*, 2017; Funatsu *et al.*, 2021).

On an interannual time scale, rainfall variability is strongly related to the ocean-atmosphere coupling modulated by anomalies of the sea surface temperatures (SST). The oceanic phenomenon most often implicated in South American precipitation variability is the El Niño Southern Oscillation (ENSO) in the Pacific, in which cold (La Niña) or warm (El Niño) phases result in rainfall excesses or deficits, depending on the region of the subcontinent (Kousky, Kagano and Cavalcanti, 1984; Aceituno, 1988; Marengo, 1992; Marengo and Espinoza, 2016; Sulca *et al.*, 2017 ; (Towner *et al.*, 2020) ; among others). However, the impact of ENSO is variable and depends on its duration, intensity, location in the eastern or central Pacific (Takahashi *et al.*, 2011; Andreoli *et al.*, 2016; Tedeschi *et al.*, 2016; Jimenez *et al.*, 2021), and its association with temperature anomalies in the tropical North and/or South Atlantic. In addition, the role of the Atlantic on the South American rainfall is increasingly highlighted. Indeed, the warming of the tropical North Atlantic is related to a lengthening of the dry season in southern Amazonia and to severe droughts in 2005 and 2010 in the Amazon basin (Marengo *et al.*, 2008; Zeng *et al.*, 2008; Marengo and Espinoza, 2016; Arias *et al.*, 2020). Moreover, Espinoza *et al.* (2014) showed that the exceptional flood of 2014 in the southwestern AB was due to warm conditions in the Indo-Pacific Ocean and a strong warm gradient between the tropical and sub-tropical South Atlantic Ocean.

On the other hand, at higher frequency, other atmospheric modes than ENSO or coupling with Atlantic SST anomalies can cause strong precipitation variability. For instance, Mayta et al. (2019) showed that around 25% of the intraseasonal rainfall extremes in the Amazon basin are related to the eastwards propagating equatorially confined Madden Julian Oscillation (MJO; Madden and Julian, 1971). Other high-frequency mechanisms such as Rossby wave trains in the Southern Hemisphere have been proposed to explain the observed intraseasonal and synoptic rainfall variability. According to these results, extratropical wind intrusions into the southern Amazon and cross-equatorial wind regimes contribute to the weather patterns variability over the Amazon basin and associated rainfall (Wang and Fu, 2002; Paccini *et al.*, 2017), including the onset and demise of the wet season in southern Amazon (Fu *et al.*, 2013; Arias *et al.*, 2015; Espinoza *et al.*, 2021).

Several previous studies have focused on rainfall patterns, their spatial and temporal diversity in the AB and their link with SST anomalies, or with the high frequency phenomena described above, most often

with an emphasis on the study of extreme events. However, few studies have been dedicated to analyzing systematically the intraseasonal regional consistency of precipitation anomalies based on long-term in-situ rainfall stations.

The present work contributes to the analysis of intra-seasonal precipitation variability. To this end, we define a "seasonal type" that is cluster of years with similar intra-seasonal rainfall variability in a regional scale. Furthermore, we aim at explaining the modulation of these seasonal types through the comparison of rainfall anomalies with those of i) cloud cover - in order to better identify the major convection regions -, ii) the IWV circulation which favor or restrict precipitation, and iii) SST, especially in the tropical and subtropical Pacific and Atlantic oceans

The paper is organized as follows: The second section presents the data used in this study. Section 3 introduces the methods used to distinguish first, homogeneous precipitation regions, then, seasonal types and relate the latter to elements of atmospheric circulation and Pacific and Atlantic SST. Finally, section 4 presents the results and discusses them before a final section with conclusion and final remarks .

II. Data

a) Daily Rain Gauge Data

Rainfall stations offer long (more than 30 years) and relatively reliable time series making it possible to analyze the temporal variability of rainfall on a small scale, despite their sparseness in the AB and possible measurement errors. Rainfall from models derived satellite data also have limitations, on the one hand the time series rarely cover three decades and although progress has been made since the first generation satellite (Fassoni-Andrade et al., 2021), rainfall estimates are still difficult to calibrate. Indeed, rainfall estimations from satellite models often tend to be overestimated. As a matter of fact, even a satellite product from TRMM 3B42, which has one of the longest estimated series and among the best quality, tend to overestimate the mean annual precipitation (Michot et al., 2018) and overestimate precipitations particularly during the rainiest season in south, north, and northeast of the AB (Michot et al., 2018) and in west and center regions during dry season (Zulkafli et al., 2014; Zubieta et al., 2015; Michot et al., 2018). Another major issue for this work is that it is not totally reliable to entirely reproduce the seasonal differences of some regions of the AB like in the Marañón and the Ucayali subcatchments. For this reason we chose to use observed data, from a network of 205 rain gauges (Figure 1) at daily scale, for which advanced quality control has been implemented (more details can be found in Michot et al., 2019). The data from the stations cover the period from 1981 to 2013 and were obtained from the National Water Agency (ANA) and the National Meteorological Institute (INMET) in Brazil, the National Meteorological and Hydrological Institute (INAMHI) in Ecuador, the Hydrological Meteorological and Environmental Studies Institute (IDEAM) in Colombia, and the respective National Meteorological and Hydrological Services (SENAMHI) in Peru and Bolivia. Unfortunately, no such data could be collected in Venezuela, and in the southwest part of the Amazon basin (between 10°S-15°S and 76°W-69°W) because data from stations in these regions did not meet the criteria for the database used for this work (more details can be found in Michot et al., 2019). The rain gauge-based data is able to account for the diversity of mean annual rainfall even though it misses the rainfall hotspots in the south and southwest of the Amazon-Andes transition zone (Espinoza et al., 2015 ; Chavez and Takahashi, 2017), as shown by the data from the Tropical Rainfall Measurement Mission (TRMM) satellite product (Figure 1).

b) Outgoing Longwave Radiation and integrated water vapor flux

Outgoing Longwave Radiation (OLR) was used as a proxy of deep convective clouds and was obtained from the National Center for Atmospheric Research of the National Ocean and Atmospheric Administration (NCAR/NOAA; Liebmann and Smith, 1996). Integrated water vapor flux (IWV) reanalysis (Kalnay *et al.*, 1996) that can provide indications about the pressure fields, is from the National Center for Environmental Prediction (NCEP-NCAR). The IWV is computed from the specific humidity and the horizontal wind (zonal - u) and meridional (v) from the ground to 300 h Pa (Peixoto and Oort, 1992; Satyamurty, da Costa and Manzi, 2013) as:

$$F_W = \int qV\, p/g \qquad (1)$$

where q is the humidity, V is the wind vector, p is the pressure, and g is the acceleration due to gravity. This is a vertically integrated value indicates whether atmospheric motions act to decrease (for divergence) or increase (for convergence) the vertical integral of moisture, over a given time period. High positive values of this parameter (i.e. large moisture convergence) can be related to precipitation intensification and floods.

c) Sea Surface Temperature data

The NOAA-CPC global monthly SST data at 2°x2° horizontal grid resolution (Smith and Reynolds, 2004) are used to analyze the variability of surface temperatures in the tropical Pacific and Atlantic oceans. The types of El Niño (EN) and La Niña (LN) events to which we refer to describe the relation between rainfall and oceanic anomalies, are detailed in Takahashi *et al. (*2011), Andreoli *et al. (*2016), Tedeschi *et al.* (2016), Pillai *et al.* (2021).

III. Methods

a) The spectral clustering method

The spectral clustering method is used in order to i) classify the stations according to their annual regime and define homogeneous rainfall regime regions in the AB, and ii) classify the years within a region to detect the seasonal types.

The main principle of spectral clustering is to represent all rain gauges in separate nodes of a connected graph whose vertexes express the similarity between two nodes. The spectral analysis of this graph graph (i.e analysis of the matrices that represent connections inside the graph) enables it to isolate its main consistent groups. To compute the connection between two nodes into this graph, the basic solution consists in computing the usual Euclidian distance. However, for clusters where the separation is tricky and non-linear, we exploit the kernel trick. It consists in projecting data in a space other than the usual one (i.e. represented by time series of rainfall) where the separation between clusters is linear. Under some specific properties (see Camps-Valls and Bruzzone, 2009 for a complete theory of kernels) this projection can simply be done by changing the way one computes the connection between nodes. In practice, this is done using a Gaussian kernel where the connection between two rain gauges x_1 and x_2 is given by:

$$K(x_1, x_2) = e^{\frac{-\|x_1 - x_2\|}{\sigma^2}} \qquad (2)$$

where σ is a parameter to fix. This kernel enables to efficiently separate highly non-linear clusters. By a non-linear separation, we refer to the idea that the boundaries that separate different clusters of rain

gauges are not linear in nature. Unlike linear separation, which assumes that clusters can be divided by straight lines or hyperplanes, non-linear separation acknowledges that clusters might be intertwined or have complex, curvy, or irregular boundaries that cannot be accurately represented by linear models. Non-linear separation is particularly important when dealing with data in high-dimensional spaces (as in our situation), where linear boundaries may not adequately capture the underlying cluster structure. The non-linear spectral clustering technique aims to uncover hidden patterns and structures of precipitations in the data, even when they are not easily distinguishable by simple linear separation.

b) Determination of homogeneous regions based on their rainfall regimes

Mean historical precipitation regimes are often computed based on a multi-decadal time series, but spatially averaging these series do not discriminate well between homogeneous and transition areas where regimes are less well individualized. Indeed, some regions may have the same year-to year variability of the seasonal regime and thus have a stronger spatial consistency, while in other regions the regime is more variable from one year to another. Our approach therefore aims to identify the areas where regimes are similar year after year. In order to do this, we first use the spectral clustering method to describe year by year the spatial distribution of rainfall regimes, from August to July of the following year, as most of the rainy seasons or wetter periods are centered on the austral summer. The geographical coordinates of the stations are not considered to avoid forcing spatial homogeneity. Indeed, even if spatial coordinates can be valuable in a clustering problem involving spatial data, in this particular situation where the goal is to obtain homogeneous groups of precipitation whatever the location, it is preferable not to use spatial coordinates to avoid introducing a bias that might cluster nearby stations together. This procedure leads to one classification per year. An open issue of data clustering for which no sound solution yet exists is the determination of the optimal number of clusters. In this study, we rely on the intra/inter inertia to obtain reliable clusters. A good clustering should indeed exhibit homogeneous data within each cluster and a large variability between different clusters (for example between the mean of each cluster). This notion of homogeneity can be quantified using the standard deviation of the data: the average of the standard deviations of the time series within each cluster gives the intra-class variance and the standard deviation between the centers of each cluster gives inter-class variance. Therefore, the ratio between the inertia among clusters and the internal inertia should be maximal. Applying this approach to each year of the series, the optimal number of clusters obtained is 13 per year. Small clusters (less than five rain gauges) are gathered with the nearest cluster (considering the spatial distance and interclass variance), in this case the number of annual clusters is reduced 10 to 6.

Finally, to analyze the pairing of the stations, i.e. to define which stations were most often part of the same cluster, we mapped the weight of the link between the stations through the time series thanks to the 'Cartography' package of the R-cran software (http://rgeomatic.hypotheses.org/659). This allowed us to visualize the sectors within which the annual regimes were most often similar. Conversely, stations with more random behavior were determined as belonging to a transition region.

c) Detection of seasonal type in a homogeneous region

Since the interannual variability of daily precipitation is very high, the intercomparison of annual patterns was achieved by performing a Fourier transform to smooth the data, removing frequencies higher than 60 days. On the one hand this frequency allows to observe, if it is the case, alternating rainfall anomalies during the season, while higher frequencies show only one anomaly direction. On the other hand, this time step may correspond to intra-seasonal atmospheric variability modes. Thus, a

smoothing of 60 days allowed us to keep a daily time step with a reduced noise so that we could observe more adequately the evolution of the annual regime of precipitation.

From these smoothed annual regimes, we identified in each region the clusters of years that have had a similar rainfall regime, which correspond to our seasonal types, using the previously described spectral clustering method. The maximum number of seasonal types is arbitrarily set at four but without imposing any minimum number. The years are as before, defined from August to July of the following year, with the exception of the Northern Region where the rainy season is aligned to the boreal summer (Rao and Hada, 1990), i.e. from June to September. The number of years within these seasonal types is very heterogeneous, a greater homogeneity between them is obtained by eliminating the least representative years in each type. Years are eliminated when their distance from the mean regime is greater than a threshold which is the sum of the mean and the standard deviation of all distances from the historical mean seasonal regime. The choice of the number of representative years, seven, was defined by the median (Stavig and Gibbons, 1977) of the number of years of all AB seasonal types. One limitation of this approach is that we cannot speak in terms of magnitude of the anomalies because of the different number of years between the seasonal types compared. Our results therefore only allow us to analyze the duration and sign of the rainfall anomalies.

d) The seasonal parameters chosen to characterize different seasonal types

The onset and demise dates of the rainy season are crucial parameters for agricultural planning, for example for determining sowing dates and whether more than one crop may be planted and harvested. In equatorial regions, for which there is no real dry season, dates delineating a wetter period were calculated.

In this study, we used the Anomalous Accumulation method developed by (Liebmann *et al.*, 2007) which is based on a threshold easily calculable for each region because it is the daily average of the series. Since the average is recalculated for each series, and here for each region, this method takes into account the local climatology (Liebmann *et al.*, 2007; Arvor *et al.*, 2014, 2017; Michot, Dubreuil and Ronchail, 2014; Dubreuil *et al.*, 2017) and allows us to catch the dates of the rainy season and their shifts. The Cumulative Anomaly Method has the great advantage of systematically providing dates at the beginning and end of the rainy season or a wetter period.

An adaptation has been realized to define the onset and demise of rainfall in the seasonal types in order to take into account a shift in their dates in relation to those of the average regional regime. The deviation from the average is not calculated in relation to the daily average of their own series but in relation to that of the region. This makes it possible to identify a deviation from the average regime of the region and not simply to identify the dates corresponding to a seasonal type.

Since it is difficult to determine thresholds for rainfall quantity the assessment of the onset and demise of the rainiest season is estimated using pentads as in Fu *et al.* (2013). The dates are therefore considered early or late when the shift exceeds one pentad, i.e. five days.

e) Relationships between rainfall and oceano-atmospheric variables

Composite of seasonal anomalies of OLR and monthly anomalies IWV are the difference between the mean value of the representative years belonging to a seasonal type and the mean value of the climatological period 1981–2013 (from August y-1 to July y) and only the significant anomalies values (higher than 2 standard deviation; (Espinoza *et al.*, 2012; Takahashi *et al.*, 2021) are considered. The precipitation anomalies are normalized, that is, divided by the standard deviation of the whole study period. Rainfall regimes and seasonal types in the AB, discussions

a) Homogeneous precipitation regions versus transition regions

Figure 2 shows the frequency of the annual pairing of the stations for the period 1981-2013. A spatial distinction becomes clearer when stations are paired 50% of the time (Figure 2 b) i.e. when they are in the same cluster half of the time. When the threshold increased to 60% (Figure 2 c), there are isolated stations assigned to a transition sector as they have roughly one chance in two to belong to one group or another. Beyond a threshold of 60% the number of linked stations falls rapidly while the number of isolated stations increases sharply. This decrease can have several explanations, including poor data coverage. Since the spatial variability of precipitation on an intra- and inter-annual scale is significant, the further apart the stations are, the less likely it is that their annual regime has been the same, and that they are therefore grouped together several times in the same annual cluster. This explains why stations with few neighbors are linked fewer times to others and are therefore isolated. However, the northeast, north, northwest and southeast of the basin form organized groups up to a threshold of 70% (Figure 2 d), indicating a greater spatial consistence of precipitation regimes in these regions. The final differentiation of the homogeneous regions results from the division of the groups of well individualized stations from there from 60%. It is important to note that these groups do not mean that all the stations are systematically linked together.

The regional classification (Figure 3) is also comparable to that provided by previous studies (Figueroa and Nobre, 1990; Espinoza Villar *et al.*, 2009; Barbosa Santos, Sérgio Lucio and Silva, 2015; Delahaye *et al.*, 2015). Tropical regions with dry season (Northeast, North, Southeast, South) are correctly distinguished from those with an equatorial climate (without dry season; Rio Negro, western Amazon). The homogeneous climatic regions based on the cluster analysis reflects well the AB intra-seasonal spatial variability, especially between the northwest and southeast of the Amazon basin, which is coherent with the eastwards propagation of the MJO described by Mayta et al. (2018).

In more detail, a distinction among the tropical regions is well made between (i) the North-East, where the maximum rainfall is observed between March and April, during the southernmost position of the Atlantic ITCZ (Espinoza et al. 2009) ; (ii) the North, with a rainy season centered in the austral winter, (iii) the South-East and the South, are grouped because of their wet season in austral season but are differentiated from each other due to their different amount of rainfall. Indeed, the incursion of extra-tropical cold fronts into the Bolivian Amazon in the austral winter (Garreaud, 2000; Seluchi and Marengo, 2000), results in greater winter rainfall in the south than in the southeast (as a proportion of annual rainfall). However, in the south, the variability of precipitation between different sectors of Bolivia (Roche *et al.*, 1990; Ronchail and Gallaire, 2006) associated with the small number of rainfall stations available for this study, leads to a fragmentation into annual clusters composed of very few stations. These were then grouped in the clusters that were spatially closest. The Andes and the Bolivian plain are thus united in the Southern region, despite the fact that rainfall variability also exists between these two sectors, as reflected in the boxplots associated with this regime in Figure 3.

In the equatorial Amazon-Andes transition zone the stations are gathered in a single region whereas a north-south split and a more pronounced bi-modal precipitation regime would have been expected (Laraque *et al.*, 2007 ; Segura et al., 2019). The unification into a single region may be related on the one hand to the fact that geographic coordinates are not taken into account in the clustering analysis (the north and south are therefore not differentiated), and the shapes of the annual distributions of the rainfall series of this region being close enough to integrate them into a common cluster. On the other hand, according to the criteria applied in our approach, the division into homogeneous regions is based on the spatial continuity of the links between the stations (Figure 2), which remains continuous at 60% and even 70%, although the links are less important between the north and the south of this Andean region. This north-south continuous homogeneity agrees with the impact of the MJO convective core

propagation from the tropical Pacific to the northwestern South America, particularly identified in the Amazon-Andes transition zones of Peru and Ecuador (Recalde-Coronel *et al*., 2020).

The South and Andes regions have the highest heterogeneity rain gauges values as implied by the scatter observed on the boxplots and the highest AB coefficient of variations values (Figure 3). The full diversity of local regimes, more rainfall in lowland than on the Altiplano, may not be represented, however, this more complex reality could only have been captured by creating a large number of regions. A better division of these areas could in principle be achieved using satellite products such as TRMM 3B42 version 7 (Arvor *et al.*, 2014; Michot *et al.*, 2018), however a long enough (three-decades) time series is not yet available.

In the northwest AB the regimes are relatively homogeneous throughout the year, however the distinction between the Rio Negro region and the West region is due to a different timing of the maxima, comprised between April and June for the Rio Negro region and between February and April for the Western region, consistent with the quarterly rainfall percentages observed by Espinoza *et al.(*2009) in the basin.

It is also regrettable that no stations were available in the south-western part of the basin (between 10°S-15°S and 76°W-69°W), where it has recently been shown that the annual variability of precipitation in the southern tropical Andes is linked to a change in the dominant mode of atmospheric circulation (Segura *et al.*, 2020). For the past fifteen years, this region has been experiencing heavier precipitation between December and February, certainly due to the strengthening of the meridional circulation between the tropical North Atlantic and tropical western South America.

b) Description of the seasonal types

The cluster analysis allowed to define subregions within the basin in which the annual rainfall cycle is spatially homogeneous. We explore now the seasonal types for each of these regions. Figure 4 shows for each region the historical mean seasonal regime (black line), the detected seasonal types (blue line), the precipitation anomalies calculated with respect to the mean seasonal regime of the region and standardized by the standard deviation of the climatology of the region (solid black) and finally, the dates of the beginning and end of the rainy season for the mean seasonal regimes (grey vertical lines) and for the seasonal types (orange vertical lines).

All regions, except the West, are characterized by 4 seasonal types. Some clusters include only one year (Figures 4b2 and 4c1) and are thus excluded as they correspond solely to an exceptional year. Furthermore, the Western region is totally excluded from the remaining of the analysis since only the anomalies of the year 1981-82 could be distinguished in a significant way whereas all the other years of the series are grouped in a single cluster. One of the reasons for this lower detection may be related to the average regime with constant precipitation during the year and that does not vary sufficiently from a year to another to be separated by the spectral clustering method and to the exceptional 1981-82 rainy season.

Rainy season dates are easily detected in the North-East, South-East, South and North where the seasonality is more pronounced (Figure 4a, 4b, 4c and 4d) and correspond to previous works (Kousky, 1988; Gan, Rao and Moscati, 2005; Vera *et al.*, 2006 a; Liebmann *et al.*, 2007). They are also consistent with the profile of the curves representing the seasonal types of the region. In the Rio Negro, although the regime is equatorial (no dry season), the onset of rainier periods detected in February is coherent with the seasonal regime. However, the demises in July seems to further correspond to the end of the defined hydrological year rather than a climatological feature.

In the Andes, the average onsets and demises dates define a long rainy season due to the bi-modal regime of the region. These dates are not obtained for the seasonal regime with deficient rainfall throughout the year (Figure 4f1 and 4f3).

Table 1 summarizes the season dates (row) and the sign of the rainfall anomalies (column) of the different seasonal types. The seasonal types mainly highlight 3 kinds of rainfall anomalies i) deficit during the whole regime ii) excess during the whole regime iii) alternating sign of the anomaly. The latter is the most frequent, corresponding to 16 out of 21 seasonal types; the rainfall anomalies often last between 30 and 60 days. It is remarkable that there are not many common years between the seasonal types of the different regions and that for the years common to the different regions, the anomalies are not the same or out of phase; there is no coherence of the seasonal types neither in time nor in space (see Figure 4).

Regarding the parameters of season dates, we note that the onset of the seasonal types have higher temporal variability (later or earlier) than demise dates, particularly in the South and Rio Negro. This higher variability in the onset dates was also found by various authors (Marengo *et al.*, 2001; Fu *et al.*, 2013; Nobre *et al.*, 2016; Arvor *et al.*, 2017) for the southern Amazon region. In general, an onset shift is not necessarily associated with a demise shift. When it occurs, an early (late) onset is most often associated with a late (early) demise and therefore with a lengthening (shortening) of the rainy season, as is the case for the seasonal type 4 in the North-East with rainfall excess during the whole regime ; for type 1 in the North with alternating signs of the rainfall anomaly; for type 4 in the South with alternating signs of the anomaly; for type 4 in the Andes with alternating signs of the anomaly. On the contrary, a late onset is most often associated with an early demise and therefore with a shortening of the rainy season, as is the case for type 1 in the North-East and type 2 in the South with deficit rainfall during the whole regime for the both types. The relationship between the date of onset and the extension of the wet season agrees with the results of Fu *et al.*, (2013) and Arvor et al. (2017) for the southern AB. The largest shifts are detected in the Rio Negro region, with an early onset of 31 days for the seasonal type 4 and a delay of 60 days for the seasonal type 1, while in the South-East, although three of the four seasonal type show onset or demise shifts, the average number of days is less important. Another important information is that a type of onset and/or demise shift is not specifically associated with a particular type of rainfall anomalies during the rainy season.

These predominant rainfall anomaly features (Figure 4 and table 1) already highlight that seasonal types with alternating anomalies are marked by the superposition of intra-seasonal and interannual variability which are difficult to disentangle and attribute to explicit drivers with large-scale or local processes. On the contrary the types with only excess or deficit of rainfall may be associated with large-scale and interannual variability drivers, for example, as a response to the interannual variability of SST.

IV. Relationships between seasonal types and SST and atmospheric circulation

We provide a detailed observed atmospheric ocean conditions for selected seasonal types in the North-East and the South-East regions. The North-East region is strongly influenced by Pacific and Atlantic conditions (Liebmann and Marengo, 2001; Gan, Kousky and Ropelewski, 2004) whereas the South-East region is influenced by the South Atlantic Convergence Zone (SACZ), which, in turn, is partially modulated by Atlantic anomalies (Liebmann *et al.*, 1999; Doyle and Barros, 2002; Taschetto and Wainer, 2008). In these regions, the seasonal type 1, 3 and 4 in the North-East and the seasonal type 3 in the South-East, are associated with specific sea surface temperature (SSTA) conditions.

Figure S1 in supplementary material shows average conditions for OLR and moisture transport circulation, for easier comparison with the anomalies shown below.

a) North-East region

The North-East is the Amazon region closest to the Atlantic ocean, and there were often observed precipitation anomalies related to cloud cover, IWV and SST anomalies (Fu *et al.*, 2001; Marengo, 2004; Tedeschi *et al.* 2016). Our analysis confirm that for all seasonal types a preponderant link between the ITCZ activity and position, and the precipitation in the region can be observed. For example, during December-February rainfall deficits of the seasonal type 1 (Figure 4a1) with 5 years and a late onset season, positive OLR anomalies are observed in Figures 5 i, j, k indicating a moderate migration of the ITCZ towards the south of the tropical Atlantic and over northeastern South America. This is related to a reduction of IWV over the AB in December and January due to weakening of the trade winds over the equatorial Atlantic, while the IWV east of the AB and south of south America strengthens (Figure 5 i, j, k). Indeed, very heavy precipitation days (that is, daily precipitation above 20 mm) have been found to be strongly and significantly anti-correlated to the vertically integrated VIMF divergence and to the upper-level (300-100 hPa) divergence, and significantly correlated with low-level (1000-850 hPa) zonal winds in northern AB (Funatsu et al. 2021). During the second rain deficit period (March to June), the composites in Figure 5 i, m, n, o show that OLR anomalies remain positive on the equatorial Atlantic while negative OLR anomalies are seen further north indicating few activity of the ITCZ or maybe its early northward migration. This early displacement could be due both to the strengthening of the southeasterly trade winds and weakening of the northeasterlies. In addition, divergence of the IWV from March over northeastern Brazil (Figure 5 l), and from May over northern AB (Figure 5 n) is observed, and the Low Level Jet (LLJ; Vera *et al.*, 2006 b) intensified in the south. As Marengo *et al.* (2012) pointed out, the relative position of the ITCZ during the rainy season plays an important role on the variability of rainfall in the AB. The atmospheric anomalies are related to El Niño events that occur 5 times out of 6 years (Table 2 and Figure 5 a, b, c). These oceanic conditions alter the circulation of Walker and Hadley cells and lead to subsidence over the northeast Amazon. During the El Niño phase, the ITCZ is positioned further north and is less active on the AB (Hastenrath and Heller, 1977; Nobre and Moura, 1984; Nobre and Shukla, 1996).

Conversely, La Niña events lead to an intensification of the ascending branch of the Walker cell over the AB and promote convection (Barichivich *et al.*, 2018; Towner *et al.* 2020; Espinoza *et al.*, 2022). La Niña phases are related to a southward migration and more active ITCZ, driving rainfall excess on the north-east region of the AB (Marengo *et al.*, 2012). In this study, the excess rainfall during all the year and a longer rainy season of the seasonal types 3 and 4 (Figure 4a3 and 4a4) seem to be highly related to La Niña (Table 2) but also to north and south Atlantic anomalies. The combination of sea surface temperature anomalies however differs between the two seasonal type. In type 3, with 2 years, a shorter La Niña phase is associated with negative SSTA in the north Atlantic (NATL) and positive SSTA in the south Atlantic (SATL), whereas the La Niña phase of type 4 lasts longer and is only combined with positive SSTA of SATL.

In more detail, the La Niña phases of the seasonal type 3 are of the eastern and central type (Table 2; Andreoli *et al.*, 2016; Tedeschi *et al.* 2016; Pillai, Ramu and Nair, 2021). Thus, the increase in cloudiness in northeastern Brazil (Figure 6 i to o) is consistent with the precipitation excesses restricted to this region and observed in May by Tedeschi et al. (2016) during La Niña east type. According to them, the strengthening of the northeasterly trade winds and the weakening of the LLJ are more characteristic of a central La Niña, which is frequently related to an increased moisture convergence in the northwestern Amazon basin and to extreme floods in the Amazon River (Espinoza *et al.*, 2013 ; Marengo *et al.*, 2013). On the other hand, the negative SST in NATL(Table 2 and Figure 6 b and c), reinforced by the strong northerly trade winds, as well as positive SSTA in SATL (Table 2, Figure 6 a and Figure S2 in Supplementary material), participate to the strong migration and maintenance southward of the ITCZ, as also observed by Wang (2004) and thus in the precipitation deficit in April then later on a late rainy season. La Niña and negative SSTA in the NATL leading to excess rainfall in the northeastern AB are consistent with descriptions by various authors (Marengo and Hastenrath, 1993; Hastenrath, 2001;

Ronchail *et al.*, 2002; Souza, Ambrizzi and Coelho, 2004), but, the precipitation excesses could be further enhanced by the presence of warm SATL anomalies as observed by Nobre and Shukla (1996) and Fontaine *et al.* (1998). Indeed, similar to Huang and Shukla (2005) we observe that positive SATL SSTA are associated with a weakening of the subtropical high and associated trade winds in the South Atlantic (Figure 6 i to l). Furthermore, the year of 2008-09, which experienced exceptional flood in the AB and which is part of this seasonal type, is also described by Marengo et al. (2012) and Espinoza et al. (2022) with La Niña and positive SSTA in the SATL, a strong shift in the ITCZ, an intensified Walker circulation enhanced IWV from NATL, and increased precipitation in the northern and western AB.

The seasonal type 4, with 7 years, seems to be highly modulated by long La Niña events (Figure 7 a to c) from August-1 to May, four of them being Central La Nina (Table 2). Cloudiness stretching over northeastern part of the Brazil and AB is consistent with the rainfall excesses described by Tedeschi et al. (2016) during central La Niña, and a stronger convergence over the northern, northeastern, and central AB, while LLJ weakens (Figure 7 i to l). On the other hand, positive SSTA (Table 2, Figure 7 c and d, and Figure S3 in Supplementary material) in the eastern equatorial Atlantic and SATL in March to May may favor convection in the ITCZ during this period and its maintenance to the south at the end of the rainy season, as confirmed by the negative OLR anomalies. The South Atlantic SSTA, which develops more from May to July (Figure S3 in Supplementary material), can then be the cause of the resumption of rainfall at the end of the rainy season. The temporality of oceanic anomalies therefore seems to strongly modulate the temporality of precipitation.

b) South-East region

In the South-East region, seasonal type 3 (Figure 4b3) with 5 years is clearly related to the regional atmospheric circulation, and in particular the SACZ, which largely modulates the rainy season in this region. Indeed, in type 3 during the rainfall excess in October-November, negative OLR anomalies are observed over southeastern AB and Brazil indicating the enhanced presence of the SACZ (Figure 8 g and h). These excess rains are related to the decrease in IWV transport to southern South America in favor of the southeast.

Concerning Pacific SSTAs, 4 central La Niña events were present among the 5 years of this seasonal type, developing as early as August but ending early in February-April (table 3 and Figure 8 a to c). Negative ENSO phases are known to increase convection in the AB. Here, the short period of excess rainfall and enhanced convection could correspond to the short duration of the La Niña events. A study by Tedeschi et al. (2016) differentiating the action of the two types of La Niña showed relatively low precipitation anomalies in the southern AB in both cases. Similar to Tedeschi et al. (2016), the IWV anomalies of this seasonal type have characteristics akin of that of a central La Niña, with convergence over the northern and northeastern AB, anticyclonic flux anomalies east of Brazil and convergence over the AB. However, the La Niña phase ends while rainfall deficits have already occurred over the region from January to April. They correspond to positive OLR anomalies (Figure 8 j to m) over the extreme southeast of the AB, especially over southeastern Brazil and indicate a weak activity of the SACZ. These deficits are related to southeasterly flux anomalies that correspond to a decrease in IWV transport from the north to the southeastern region, where an anticyclonic-type anomaly is emerging, and a weakening of the SACZ. On the other hand, the flux anomalies supplying the ITCZ move towards the eastern SATL. This configuration continues through March and persists over the southern AB into April, explaining the early demise of the rainy season (Figure 4b3). Positive SSTA near the Brazilian coast from January to April (Figure 8 b, c and Figure S4 in Supplementary material) could help explain the occurrence of these atmospheric and precipitation anomalies while the La Niña phase is underway. It is possible that the Atlantic SSTA reflect a weakening of the eastern branch of the South Atlantic High and thus a weakening of the easterly flux, resulting in a weakened SACZ. These observations seem to be consistent with those of Doyle and Barros (2002) who show a less active SACZ in relation to strengthened IWV

towards South America and positive SSTA between 10 and 40°S, from the South American coast to 10°E. Moreover, Taschetto and Wainer (2008) indicate that the influence of the SSTA between 20 and 60°S in the Atlantic takes precedence over that of ENSO and modulates the position and intensity of the SACZ especially between December and February. Finally, positive SSTA east of SATL (table 3 and Figure 8 c), from February to April, could further explain the significant activity of the ITCZ over the Atlantic, the deflection of the flux east of SATL and the early demise of the rainy season in the Southeast region.

Discussion and conclusion

This analysis was performed using data from 205 rain gauges, based on which the spectral clustering method and geomatic tool allowed us to obtain seven homogeneous precipitation regions separated by transition areas, and then, within each region to detect clusters of years with similar rainfall regimes, which we referred to as seasonal types. The seven region revealed in this study show for example the separation between regions with or without dry seasons, between highlands and lowlands and between west and east. These regions also reflect the eastwards propagation of the MJO described by previous studies over the Amazon basin.

The seasonal types detected can be summarized by three kinds of rainfall anomalies i) deficit during the whole year ii) excess during the whole year iii) alternating sign of the anomaly, which is the most frequent type. We found that the lag of the onset or demise rainy season dates are not associated with specific rainfall anomaly. Furthermore, the onsets of the seasonal types are more often shifted to later or earlier (than the mean average date) than demise dates, particularly in the South and Rio Negro basin (northern Amazonia). A demise shift does not appear associated with an onset shift. When it occurs, an early (late) onset is most often associated with a late (early) demise, and therefore with a lengthening (shortening) of the rainy season.

IWV and OLR anomalies are generally consistent with the rainfall anomalies characterizing each seasonal types. In addition, in the North-East and South-East, some seasonal types are associated with SSTA in the tropical Pacific and Atlantic, that can help to understand a part of the interannual precipitation variability. In the North-East, as already showed in the literature, we confirmed the close relationship between precipitations anomalies and the ITCZ intensity and displacement. In this region, seasonal type corresponding to dry and shorter rainy seasons are frequently associated to El Niño events (mainly in central and some in the eastern Pacific), when the ITCZ moves less southwards and is less active. Conversely, longer rainy season is observed when La Niña events occur. However the influence of the Atlantic SSTA is noticeable, as they also are responsible for a longer rainy season, while rainfall anomalies vary depending on timing and signal of these SSTA. When the South Atlantic SSTA are positive, rainfalls remain in excess, however, when SSTA are positive in the South Atlantic and negative on the North Atlantic, rainfall anomalies are contrasted.

In the South-East the more relevant links between atmospheric and oceanic anomalies were observed for the seasonal types with alternating anomalies and an early demise of the rainy season. During La Niña conditions we observed at the beginning of the rainy season a more active SACZ and an excess of rainfall. During the rainy seasonal types rainfall deficits occur when the SACZ is weak because of a decrease of the IWV from the north and an anticyclonic anomaly of these flux in the region and South-East Brazil. These rainfall deficits and the weakening of the south Atlantic High and the SACZ could be related to positive SSTA near the Brazilian coast, which is consistent with the observations of previous studies. A relevant point to notice is that the temporality of the onset and demise of oceanic anomalies seems to strongly modulate the temporality of precipitation anomalies, as shown in previous studies (Tomasella *et* al. 2010; Marengo *et* al. 2012; Espinoza *et* al. 2013).

This article thus helps to summarize the diversity of regional rainy season types that can occur in Amazonia. Oceanic conditions can explain a part of the interannual rainfall variability, however, the superposition with intra-seasonal processes of rainfall variability remain a major issue to predict the precipitation anomalies (e.g. Mayta et al., 2019). That is why there is a need to continue to explore and understand the weight of the different factors behind these patterns of variability. First, for a better interpretation of the SSTA role on convection and IWV anomalies and on the precipitation of these seasonal types, it will be necessary to expand the analysis using complementary variables such as vertical motions in the atmosphere and divergence/convergence fields. Furthermore, we will need to determine the drivers that influence intra-seasonal variability and in particular to investigate the role of the MJO in modulating regional rainfall anomalies for each seasonal types here. This is relevant since it is known that MJO can have significantly affect seasonal rainfall in the tropics (Zhang 2005), especially in the SACZ area (Carvalho *et al.*, 2004, Nogués-Paegle *et al.* 2000), and including extremes over the Amazon basin (Mayta et al., 2019) and tropical South America (Recarlde-Coronel et al., 2020).

Our results also suggest a relevant role of local scale in modulating seasonal types. Therefore, we need to formulate some hypothesis, from land use changes (Debortoli et al., 2017; Arvor et al., 2017, Wongchuig et al., 2021., among others) to complex topography, mainly in Andean countries (Espinoza et al., 2015, Chavez and Takahashi 2017; Junquas et al., 2018). Certainly many other environmental parameters could contribute to influence the dates of the rainy season and rainfall anomalies (Fu *et al.*, 2013; Yin *et al.*, 2014; Arias et al., 2020) among them, previous dry season conditions are increasingly pointed to as factors directly influencing the mechanisms of transition to the wet season, and thus the shift in the demise of the rainy season (Yin *et al.*, 2014; Marengo *et al.*, 2022).

Thus, seasonal types provide an understanding of how rainfall patterns vary in the Amazon basin and are the first step in improving seasonal predictability. However, accurate prediction also depends on a good understanding of how multiscale factors modulate seasonal types which will be the subject of the next step.

Acknowledgments The authors would like to express their thanks to the University of Rennes 2 which provided a doctoral fellowship that made this work possible, and T. Giraud from the RIATE, for his precious guidelines on the use of the Cartography package. J.C Espinoza has been supported by the French AMANECER-MOPGA project funded by ANR and IRD (ref. ANR18-MPGA-0008).

Data availability statement Data available on requeston from the authors.

References

Aceituno, P. (1988) 'On the Functioning of the Southern Oscillation in the South American Sector. Part I: Surface Climate', *Monthly Weather Review*, 116(3), pp. 505–524. Available at: https://doi.org/10.1175/1520-0493(1988)116<0505:OTFOTS>2.0.CO;2.

Andreoli, R.V. *et al.* (2016) 'The influence of different El Niño types on the South American rainfall', *International Journal of Climatology*, p. n/a-n/a. Available at: https://doi.org/10.1002/joc.4783.

Arias, P.A. *et al.* (2015) 'A correlated shortening of the North and South American monsoon seasons in the past few decades', *Climate Dynamics*, 45(11), pp. 3183–3203. Available at: https://doi.org/10.1007/s00382-015-2533-1.

Arias, P.A. *et al.* (2020) 'Changes in Normalized Difference Vegetation Index in the Orinoco and Amazon River Basins: Links to Tropical Atlantic Surface Temperatures', *Journal of Climate*, 33(19), pp. 8537–8559. Available at: https://doi.org/10.1175/JCLI-D-19-0696.1.

Arvor, D. *et al.* (2014) 'Spatial patterns of rainfall regimes related to levels of double cropping agriculture systems in Mato Grosso (Brazil): Spatial patterns of rainfall regimes in Mato Grosso', *International Journal of Climatology*, 34(8). Available at: https://doi.org/10.1002/joc.3863.

Arvor, D. *et al.* (2017) 'Monitoring Rainfall Patterns in the Southern Amazon with PERSIANN-CDR Data: Long-Term Characteristics and Trends', *Remote Sensing*, 9(9), p. 889.

Barbosa Santos, E., Sérgio Lucio, P. and Silva, C.M. (2015) 'Precipitation regionalization of the Brazilian Amazon', *Atmospheric Science Letters*, 16(3), pp. 185–192.

Barichivich, J. *et al.* (2018) 'Recent intensification of Amazon flooding extremes driven by strengthened Walker circulation', *Science Advances*, 4(9), p. eaat8785. Available at: https://doi.org/10.1126/sciadv.aat8785.

Camps-Valls, G. and Bruzzone, L. (2009) *Kernel Methods for Remote Sensing Data Analysis | Wiley*. Wiley.

Carvalho, L.M.V., Jones, C. and Liebmann, B. (2004) 'The South Atlantic Convergence Zone: Intensity, Form, Persistence, and Relationships with Intraseasonal to Interannual Activity and Extreme Rainfall', *Journal of Climate*, 17(1), pp. 88–108. Available at: https://doi.org/10.1175/1520-0442(2004)017<0088:TSACZI>2.0.CO;2.

Chavez, S.P. and Takahashi, K. (2017) 'Orographic rainfall hot spots in the Andes-Amazon transition according to the TRMM precipitation radar and in situ data', *Journal of Geophysical Research: Atmospheres*, 122(11), pp. 5870–5882. Available at: https://doi.org/10.1002/2016JD026282.

Delahaye, F. *et al.* (2015) 'A consistent gauge database for daily rainfall analysis over the Legal Brazilian Amazon', *Journal of Hydrology*, 527, pp. 292–304.

Doyle, M.E. and Barros, V.R. (2002) 'Midsummer Low-Level Circulation and Precipitation in Subtropical South America and Related Sea Surface Temperature Anomalies in the South Atlantic', *Journal of Climate*, 15(23), pp. 3394–3410. Available at: https://doi.org/10.1175/1520-0442(2002)015<3394:MLLCAP>2.0.CO;2.

Dubreuil, V. *et al.* (2017) 'Local rainfall trends and their perceptions by Amazonian communities', *Climatic Change*, 143(3), pp. 461–472. Available at: https://doi.org/10.1007/s10584-017-2006-0.

Espinoza, J.C. *et al.* (2012) 'The Major Floods in the Amazonas River and Tributaries (Western Amazon Basin) during the 1970–2012 Period: A Focus on the 2012 Flood', *Journal of Hydrometeorology*, 14(3), pp. 1000–1008. Available at: https://doi.org/10.1175/JHM-D-12-0100.1.

Espinoza, J.C. *et al.* (2014) 'The extreme 2014 flood in south-western Amazon basin: the role of tropical-subtropical South Atlantic SST gradient', *Environmental Research Letters*, 9(12), p. 124007. Available at: https://doi.org/10.1088/1748-9326/9/12/124007.

Espinoza, J.C. *et al.* (2015) 'Rainfall hotspots over the southern tropical Andes: Spatial distribution, rainfall intensity, and relations with large-scale atmospheric circulation', *Water Resources Research*, 51(5), pp. 3459–3475. Available at: https://doi.org/10.1002/2014WR016273.

Espinoza, J.-C. *et al.* (2021) 'Recent Changes in the Atmospheric Circulation Patterns during the Dry-to-Wet Transition Season in South Tropical South America (1979–2020): Impacts on Precipitation and Fire Season', *Journal of Climate*, 34(22), pp. 9025–9042. Available at: https://doi.org/10.1175/JCLI-D-21-0303.1.

621 Espinoza, J.-C. *et al.* (2022) 'The new historical flood of 2021 in the Amazon River compared to major
622 floods of the 21st century: Atmospheric features in the context of the intensification of floods',
623 *Weather and Climate Extremes*, 35, p. 100406. Available at:
624 https://doi.org/10.1016/j.wace.2021.100406.

625 Espinoza Villar, J.C. *et al.* (2009) 'Spatio-temporal rainfall variability in the Amazon basin countries
626 (Brazil, Peru, Bolivia, Colombia, and Ecuador)', *International Journal of Climatology*, 29(11), pp. 1574–
627 1594.

628 Fassoni-Andrade, A.C. *et al.* (2021) 'Amazon Hydrology From Space: Scientific Advances and Future
629 Challenges', *Reviews of Geophysics*, 59(4), p. e2020RG000728. Available at:
630 https://doi.org/10.1029/2020RG000728.

631 Figueroa, S.N. and Nobre, C.A. (1990) 'Precipitation distribution over central and western tropical
632 South America', *Climanalise*, 5(6), pp. 36–45.

633 Fontaine, B. *et al.* (1998) 'Anomalies de température de surface de la mer et précipitations tropicales
634 synthèse de quelques travaux récents portant sur les précipitations au Sahel et dans le Nordeste'.
635 Available at: http://documents.irevues.inist.fr/handle/2042/47056 (Accessed: 29 December 2016).

636 Fu, R. *et al.* (2001) 'How do tropical sea surface temperatures influence the seasonal distribution of
637 precipitation in the equatorial Amazon?', *Journal of Climate*, 14(20), pp. 4003–4026.

638 Fu, R. *et al.* (2013) 'Increased dry-season length over southern Amazonia in recent decades and its
639 implication for future climate projection', *Proceedings of the National Academy of Sciences*, 110(45),
640 pp. 18110–18115.

641 Funatsu, B.M. *et al.* (2021) 'Assessing precipitation extremes (1981–2018) and deep convective
642 activity (2002–2018) in the Amazon region with CHIRPS and AMSU data', *Climate Dynamics*, 57(3),
643 pp. 827–849. Available at: https://doi.org/10.1007/s00382-021-05742-8.

644 Gan, M.A., Kousky, V.E. and Ropelewski, C.F. (2004) 'The South America Monsoon Circulation and Its
645 Relationship to Rainfall over West-Central Brazil', *Journal of Climate*, 17(1), pp. 47–66. Available at:
646 https://doi.org/10.1175/1520-0442(2004)017<0047:TSAMCA>2.0.CO;2.

647 Gan, M.A., Rao, V.B. and Moscati, M.C.L. (2005) 'South American monsoon indices', *Atmospheric
648 Science Letters*, 6(4), pp. 219–223. Available at: https://doi.org/10.1002/asl.119.

649 Garreaud, R. (2000) 'Cold Air Incursions over Subtropical South America: Mean Structure and
650 Dynamics', *Monthly Weather Review*, 128(7), pp. 2544–2559. Available at:
651 https://doi.org/10.1175/1520-0493(2000)128<2544:CAIOSS>2.0.CO;2.

652 Hastenrath, S. (2001) 'In search of zonal circulations in the equatorial Atlantic sector from the NCEP–
653 NCAR reanalysis', *International Journal of Climatology*, 21(1), pp. 37–47.

654 Hastenrath, S. and Heller, L. (1977) 'Dynamics of climatic hazards in northeast Brazil', *Quarterly
655 Journal of the Royal Meteorological Society*, 103(435), pp. 77–92.

656 Huang, B. and Shukla, J. (2005) 'Ocean–Atmosphere Interactions in the Tropical and Subtropical
657 Atlantic Ocean', *Journal of Climate*, 18(11), pp. 1652–1672. Available at:
658 https://doi.org/10.1175/JCLI3368.1.

659 Jimenez, J.C. *et al.* (2021) 'The role of ENSO flavours and TNA on recent droughts over Amazon
660 forests and the Northeast Brazil region', *International Journal of Climatology*, 41(7), pp. 3761–3780.
661 Available at: https://doi.org/10.1002/joc.6453.

662 Kalnay, E. *et al.* (1996) 'The NCEP/NCAR 40-Year Reanalysis Project', *Bulletin of the American*
663 *Meteorological Society*, 77(3), pp. 437–472. Available at: https://doi.org/10.1175/1520-
664 0477(1996)077<0437:TNYRP>2.0.CO;2.

665 Kousky, V.E. (1988) 'Pentad outgoing longwave radiation climatology for the South American sector',
666 *Revista Brasileira de Meteorologia*, 3(1), pp. 217–231.

667 Kousky, V.E., Kagano, M.T. and Cavalcanti, I.F. (1984) 'A review of the Southern Oscillation: oceanic-
668 atmospheric circulation changes and related rainfall anomalies', *Tellus A*, 36(5), pp. 490–504.

669 Laraque, A. *et al.* (2007) 'Heterogeneous Distribution of Rainfall and Discharge Regimes in the
670 Ecuadorian Amazon Basin', *Journal of Hydrometeorology*, 8(6), pp. 1364–1381.

671 Liebmann, B. *et al.* (1999) 'Submonthly convective variability over South America and the South
672 Atlantic convergence zone', *Journal of climate*, 12(7), pp. 1877–1891.

673 Liebmann, B. *et al.* (2007) 'Onset and end of the rainy season in South America in observations and
674 the ECHAM 4.5 atmospheric general circulation model', *Journal of Climate*, 20(10), pp. 2037–2050.

675 Liebmann, B. and Marengo, J. (2001) 'Interannual variability of the rainy season and rainfall in the
676 Brazilian Amazon Basin', *Journal of Climate*, 14(22), pp. 4308–4318.

677 Liebmann, B. and Smith, A.C. (1996) 'Description of a complete (interpolated) outgoing longwave
678 radiation dataset', *Bull. Amer. Meteor. Soc.*, 77, pp. 1275–1277.

679 Madden, R.A. and Julian, P.R. (1971) 'Detection of a 40-50 day oscillation in the zonal wind in the
680 tropical Pacific', *Journal of the Atmospheric Sciences*, 28(5), pp. 702–708.

681 Marengo, J.A. (1992) 'Interannual variability of surface climate in the Amazon basin', *International*
682 *Journal of Climatology*, 12(8), pp. 853–863.

683 Marengo, J.A. *et al.* (2001) 'Onset and End of the Rainy Season in the Brazilian Amazon Basin', *Journal*
684 *of Climate*, 14(5), pp. 833–852. Available at: https://doi.org/10.1175/1520-
685 0442(2001)014<0833:OAEOTR>2.0.CO;2.

686 Marengo, J.A. (2004) 'Interdecadal variability and trends of rainfall across the Amazon basin',
687 *Theoretical and applied climatology*, 78(1–3), pp. 79–96.

688 Marengo, J.A. *et al.* (2008) 'The drought of Amazonia in 2005', *Journal of Climate*, 21(3), pp. 495–516.

689 Marengo, J.A. *et al.* (2012) 'Recent developments on the South American monsoon system',
690 *International Journal of Climatology*, 32(1), pp. 1–21. Available at: https://doi.org/10.1002/joc.2254.

691 Marengo, J.A. *et al.* (2013) 'Two Contrasting Severe Seasonal Extremes in Tropical South America in
692 2012: Flood in Amazonia and Drought in Northeast Brazil', *Journal of Climate*, 26(22), pp. 9137–9154.
693 Available at: https://doi.org/10.1175/JCLI-D-12-00642.1.

694 Marengo, J.A. *et al.* (2022) 'Increased climate pressure on the agricultural frontier in the Eastern
695 Amazonia–Cerrado transition zone', *Scientific Reports*, 12(1), p. 457. Available at:
696 https://doi.org/10.1038/s41598-021-04241-4.

697 Marengo, J.A. and Espinoza, J.C. (2016) 'Extreme seasonal droughts and floods in Amazonia: causes,
698 trends and impacts', *International Journal of Climatology*, 36(3), pp. 1033–1050. Available at:
699 https://doi.org/10.1002/joc.4420.

700 Marengo, J.A. and Hastenrath, S. (1993) 'Case Studies of Extreme Climatic Events in the Amazon
701 Basin', *Journal of Climate*, 6(4), pp. 617–627.

702 Mayta, V.C. *et al.* (2019) 'The role of the Madden–Julian oscillation on the Amazon Basin
703 intraseasonal rainfall variability', *International Journal of Climatology*, 39(1), pp. 343–360. Available
704 at: https://doi.org/10.1002/joc.5810.

705 Michot, V. *et al.* (2018) 'Performance of TRMM TMPA 3B42 V7 in Replicating Daily Rainfall and
706 Regional Rainfall Regimes in the Amazon Basin (1998–2013)', *Remote Sensing*, 10(12), p. 1879.
707 Available at: https://doi.org/10.3390/rs10121879.

708 Michot, V. *et al.* (2019) 'Validation and reconstruction of rain gauge–based daily time series for the
709 entire Amazon basin', *Theoretical and Applied Climatology*, 138(1), pp. 759–775. Available at:
710 https://doi.org/10.1007/s00704-019-02832-w.

711 Michot, V., Dubreuil, V. and Ronchail, J. (2014) 'VARIABILITE INTERANNUELLE DES DATES DE DEBUT
712 ET DE FIN DE LA SAISON DES PLUIES DANS L'ARC DE DEFORESTATION AMAZONIEN.', in *XXVIIe*
713 *Colloque de l'Association Internationale de Climatologie*. Dijon, France, pp. 212–218.

714 Moron, V., Camberlin, P. and Robertson, A.W. (2013) 'Extracting subseasonal scenarios: an
715 alternative method to analyze seasonal predictability of regional-scale tropical rainfall', *Journal of*
716 *Climate*, 26(8), pp. 2580–2600.

717 Nobre, C.A. *et al.* (2016) 'Land-use and climate change risks in the Amazon and the need of a novel
718 sustainable development paradigm', *Proceedings of the National Academy of Sciences*, 113(39), pp.
719 10759–10768. Available at: https://doi.org/10.1073/pnas.1605516113.

720 Nobre, P. and Moura, A.D. (1984) 'Large scale tropical heat sources and global atmospheric energy
721 propagation associated with droughts in Northeast Brazil', in. *Presented at the WMO Symposium on*
722 *Meteorological Aspects of Tropical Droughts*, Fortaleza-Brésil.

723 Nobre, P. and Shukla, J. (1996) 'Variations of sea surface temperature, wind stress, and rainfall over
724 the tropical Atlantic and South America', *Journal of Climate*, 9(10), pp. 2464–2479.

725 Paccini, L. *et al.* (2018) 'Intra-seasonal rainfall variability in the Amazon basin related to large-scale
726 circulation patterns: a focus on western Amazon-Andes transition region: INTRA-SEASONAL RAINFALL
727 VARIABILITY IN WESTERN AMAZON', *International Journal of Climatology*, 38(5), pp. 2386–2399.
728 Available at: https://doi.org/10.1002/joc.5341.

729 Peixoto, J.P. and Oort, A.H. (1992) *Physics of climate*. New York: American Institute of Physics.

730 Pillai, P.A., Ramu, D.A. and Nair, R.C. (2021) 'Recent changes in the major modes of Asian summer
731 monsoon rainfall: influence of ENSO-IOD relationship', *Theoretical and Applied Climatology*, 143(3),
732 pp. 869–881. Available at: https://doi.org/10.1007/s00704-020-03454-3.

Rao, V.B. and Hada, K. (1990) 'Characteristics of rainfall over Brazil: Annual variations and connections with the Southern Oscillation', *Theoretical and Applied Climatology*, 42(2), pp. 81–91. Available at: https://doi.org/10.1007/BF00868215.

Recalde-Coronel, G.C., Zaitchik, B. and Pan, W.K. (2020) 'Madden–Julian oscillation influence on sub-seasonal rainfall variability on the west of South America', *Climate Dynamics*, 54(3), pp. 2167–2185. Available at: https://doi.org/10.1007/s00382-019-05107-2.

Roche, M.A. *et al.* (1990) 'Hétérogénéité des précipitations sur la cordillère des Andes boliviennes', in *Hydrology in Mountainous Regions. I-Hydrological Measurements; the Water Cycle. IAHS*. *International Conference on Water Resources in Mountainous Regions*, Lausanne-Suisse: International Association of Hydrological Sciences-IAHS, pp. 381–388.

Ronchail, J. *et al.* (2002) 'Interannual rainfall variability in the Amazon basin and sea-surface temperatures in the equatorial Pacific and the tropical Atlantic Oceans', *International Journal of Climatology*, 22(13), pp. 1663–1686. Available at: https://doi.org/10.1002/joc.815.

Ronchail, J. and Gallaire, R. (2006) 'ENSO and rainfall along the Zongo valley (Bolivia) from the Altiplano to the Amazon basin', *International Journal of Climatology*, 26(9), pp. 1223–1236.

Satyamurty, P., da Costa, C.P.W. and Manzi, A.O. (2013) 'Moisture source for the Amazon Basin: a study of contrasting years', *Theoretical and Applied Climatology*, 111(1), pp. 195–209. Available at: https://doi.org/10.1007/s00704-012-0637-7.

Segura, H. *et al.* (2019) 'New insights into the rainfall variability in the tropical Andes on seasonal and interannual time scales', *Climate Dynamics*, 53(1), pp. 405–426. Available at: https://doi.org/10.1007/s00382-018-4590-8.

Segura, H. *et al.* (2020) 'Recent changes in the precipitation-driving processes over the southern tropical Andes/western Amazon', *Climate Dynamics*, 54(5), pp. 2613–2631. Available at: https://doi.org/10.1007/s00382-020-05132-6.

Seluchi, M.E. and Marengo, J.A. (2000) 'Tropical–midlatitude exchange of air masses during summer and winter in South America: climatic aspects and examples of intense events', *International Journal of Climatology*, 20(10), pp. 1167–1190.

Smith, T.M. and Reynolds, R.W. (2004) 'Improved Extended Reconstruction of SST (1854–1997)', *Journal of Climate*, 17(12), pp. 2466–2477. Available at: https://doi.org/10.1175/1520-0442(2004)017<2466:IEROS>2.0.CO;2.

Souza, E., Ambrizzi, T. and Coelho, C.A.S. (2004) 'Two ENSO episodes with reversed impacts on the regional precipitation of the northeastern South America', *Meteorologica*, 29(1–2), pp. 5–16.

Stavig, G.R. and Gibbons, J.D. (1977) 'Comparing the Mean and the Median as Measures of Centrality', *International Statistical Review / Revue Internationale de Statistique*, 45(1), pp. 63–70. Available at: https://doi.org/10.2307/1403004.

Sulca, J. *et al.* (2017) 'Impacts of different ENSO flavors and tropical Pacific convection variability (ITCZ, SPCZ) on austral summer rainfall in South America, with a focus on Peru', *International Journal of Climatology* [Preprint]. Available at: https://doi.org/10.1002/joc.5185.

771 Takahashi, K. *et al.* (2011) 'ENSO regimes: Reinterpreting the canonical and Modoki El Niño',
772 *Geophysical Research Letters*, 38(10), p. L10704. Available at:
773 https://doi.org/10.1029/2011GL047364.

774 Takahashi, N. *et al.* (2021) 'Formation Mechanism of Warm SST Anomalies in 2010s Around Hawaii',
775 *Journal of Geophysical Research: Oceans*, 126(11), p. e2021JC017763. Available at:
776 https://doi.org/10.1029/2021JC017763.

777 Taschetto, A.S. and Wainer, I. (2008) 'The impact of the subtropical South Atlantic SST on South
778 American precipitation', *Annales Geophysicae*, 26(11), pp. 3457–3476. Available at:
779 https://doi.org/10.5194/angeo-26-3457-2008.

780 Tedeschi, R.G., Grimm, A.M. and Cavalcanti, I.F.A. (2016) 'Influence of Central and East ENSO on
781 precipitation and its extreme events in South America during austral autumn and winter',
782 *International Journal of Climatology*, 36(15), pp. 4797–4814. Available at:
783 https://doi.org/10.1002/joc.4670.

784 Towner, J. *et al.* (2020) 'Attribution of Amazon floods to modes of climate variability: A review',
785 *Meteorological Applications*, 27(5), p. e1949. Available at: https://doi.org/10.1002/met.1949.

786 Vera, C., Baez, J., *et al.* (2006) 'The South American Low-Level Jet Experiment', *Bulletin of the*
787 *American Meteorological Society*, 87(1), pp. 63–78. Available at: https://doi.org/10.1175/BAMS-87-1-
788 63.

789 Vera, C., Higgins, W., *et al.* (2006) 'Toward a Unified View of the American Monsoon Systems',
790 *Journal of Climate*, 19(20), pp. 4977–5000. Available at: https://doi.org/10.1175/JCLI3896.1.

791 Wang, C. (2004) 'ENSO, Atlantic climate variability, and the Walker and Hadley circulations', in *The*
792 *Hadley circulation: Present, past and future*. Springer, pp. 173–202. Available at:
793 http://link.springer.com/10.1007/978-1-4020-2944-8_7 (Accessed: 29 December 2016).

794 Wang, H. and Fu, R. (2002) 'Cross-Equatorial Flow and Seasonal Cycle of Precipitation over South
795 America', *Journal of Climate*, 15(13), pp. 1591–1608. Available at: https://doi.org/10.1175/1520-
796 0442(2002)015<1591:CEFASC>2.0.CO;2.

797 Yin, L. *et al.* (2014) 'What controls the interannual variation of the wet season onsets over the
798 Amazon?', *Journal of Geophysical Research: Atmospheres*, 119(5), pp. 2314–2328.

799 Zeng, N. *et al.* (2008) 'Causes and impacts of the 2005 Amazon drought', *Environmental Research*
800 *Letters*, 3(1), p. 014002.

801 Zubieta, R. *et al.* (2015) 'Impacts of satellite-based precipitation datasets on rainfall–runoff modeling
802 of the Western Amazon basin of Peru and Ecuador', *Journal of Hydrology*, 528, pp. 599–612.
803 Available at: https://doi.org/10.1016/j.jhydrol.2015.06.064.

804 Zulkafli, Z. *et al.* (2014) 'A comparative performance analysis of TRMM 3B42 (TMPA) versions 6 and 7
805 for hydrological applications over Andean–Amazon River basins', *Journal of Hydrometeorology*, 15(2),
806 pp. 581–592.

807

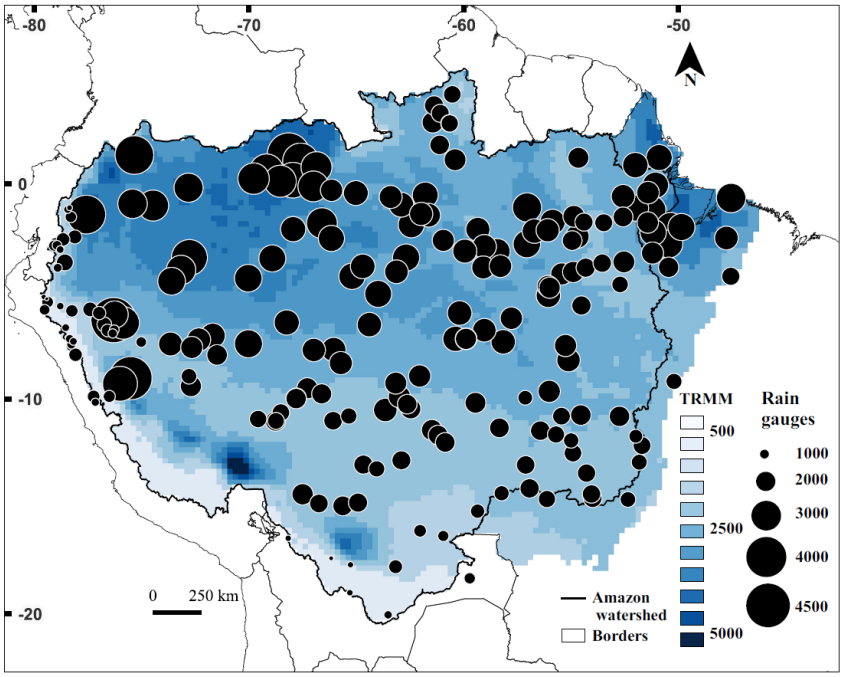

Figure 1 Annual mean rainfall in millimeters for the Amazon basin from TRMM B42 v7 (1998-2013) in blue and, from network rain gauges (1981-2013) represented by the proportional circles.

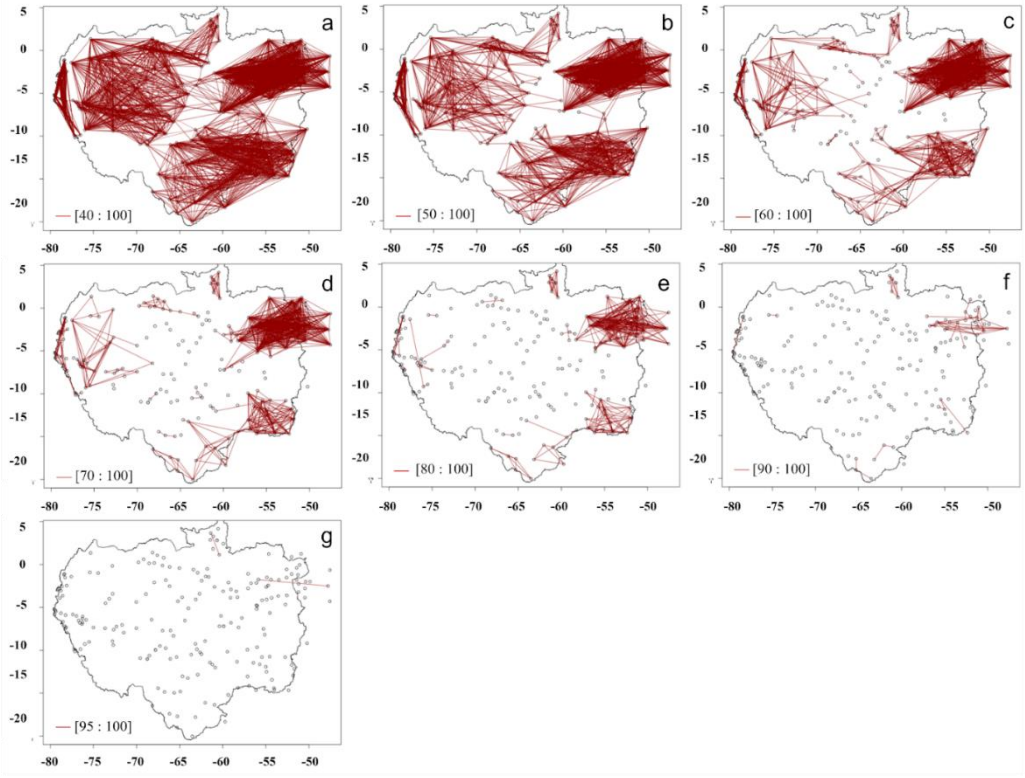

Figure 2 Frequency of paired stations for the period 1981-2013 at least a) 40% of the time, b) 50% of the time, c) 60% of the time, d)70% of the time, e) 80% of the time, f) 90% of the time, and g) 95% of the time. The gray dots represent the rain gauge stations and the red lines materialize matching between two stations.

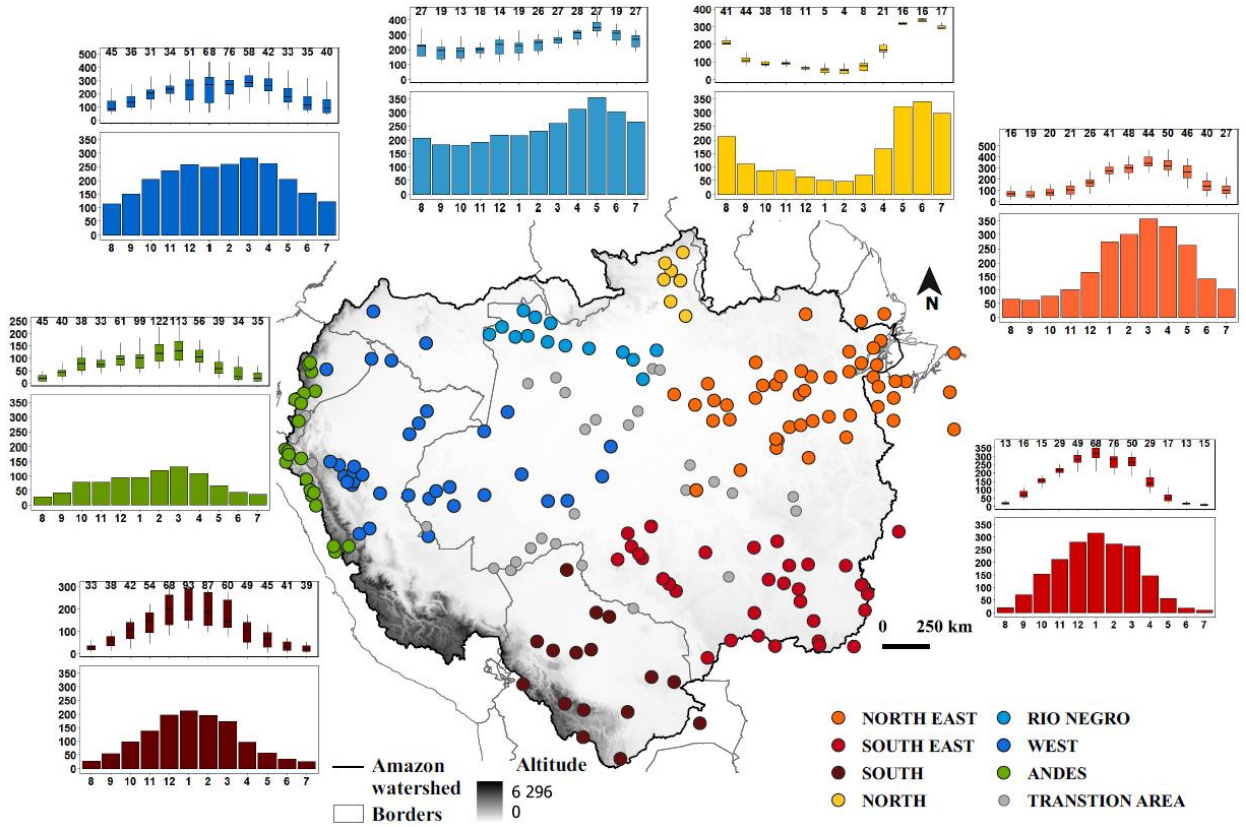

Figure 3 Map of homogeneous rainfall regions, with the same average rainfall regime, and transition areas (grey dots) in the Amazon basin based on spectral clustering method and results on Figure 2. The regions are formed from the stations that are grouped in at least 60% of the times in the same annual cluster (1981-2013). The graphics show per region the historical mean seasonal regime from August y-1 to July y (axis x) and the monthly dispersion of the station values ; the y-axis is expressed in mm. The values above the boxplots express the coefficients of variation.

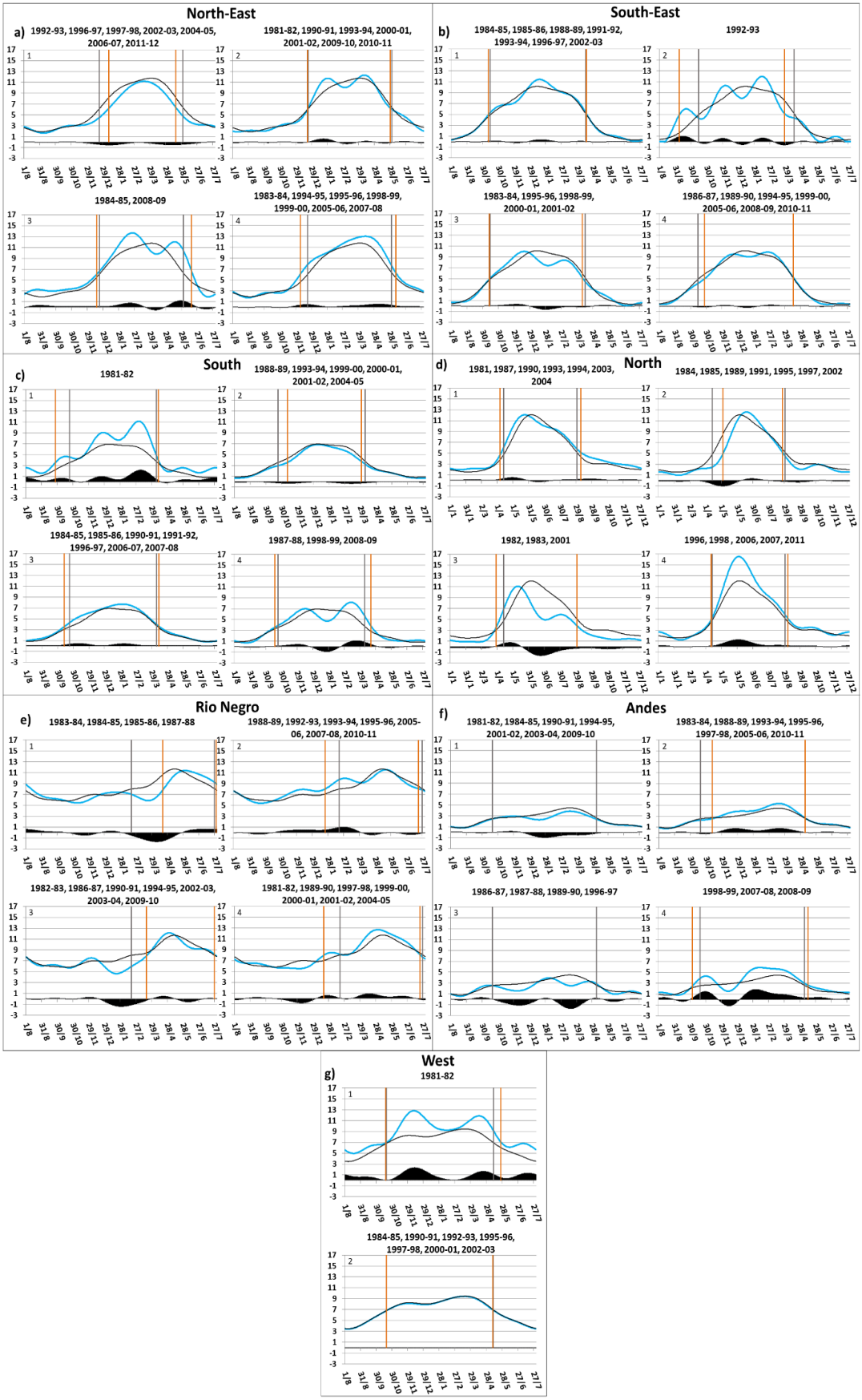
North-East
a) 1992-93, 1996-97, 1997-98, 2002-03, 2004-05, 2006-07, 2011-12
1981-82, 1990-91, 1993-94, 2000-01, 2001-02, 2009-10, 2010-11
1984-85, 2008-09
1983-84, 1994-95, 1995-96, 1998-99, 1999-00, 2005-06, 2007-08
South-East
b) 1984-85, 1985-86, 1988-89, 1991-92, 1993-94, 1996-97, 2002-03
1992-93
1983-84, 1995-96, 1998-99, 2000-01, 2001-02
1986-87, 1989-90, 1994-95, 1999-00, 2005-06, 2008-09, 2010-11
South
c) 1981-82
1988-89, 1993-94, 1999-00, 2000-01, 2001-02, 2004-05
1984-85, 1985-86, 1990-91, 1991-92, 1996-97, 2006-07, 2007-08
1987-88, 1998-99, 2008-09
North
d) 1981, 1987, 1990, 1993, 1994, 2003, 2004
1984, 1985, 1989, 1991, 1995, 1997, 2002
1982, 1983, 2001
1996, 1998 , 2006, 2007, 2011
Rio Negro
e) 1983-84, 1984-85, 1985-86, 1987-88
1988-89, 1992-93, 1993-94, 1995-96, 2005-06, 2007-08, 2010-11
1982-83, 1986-87, 1990-91, 1994-95, 2002-03, 2003-04, 2009-10
1981-82, 1989-90, 1997-98, 1999-00, 2000-01, 2001-02, 2004-05
Andes
f) 1981-82, 1984-85, 1990-91, 1994-95, 2001-02, 2003-04, 2009-10
1983-84, 1988-89, 1993-94, 1995-96, 1997-98, 2005-06, 2010-11
1986-87, 1987-88, 1989-90, 1996-97
1998-99, 2007-08, 2008-09
West
g) 1981-82
1984-85, 1990-91, 1992-93, 1995-96, 1997-98, 2000-01, 2002-03

Figure 4. 1 to 4 seasonal types detected in the a) North East, b) South East c) South d) North e) Rio Negro f) Andes and g) West regions of the Amazon basin. Years of each seasonal type are indicated above each graph. The black line represents the average precipitation regime of the region (1981-2013), the blue line the seasonal type, and solid black the precipitation anomalies (blue line minus black line). The abscissae are expressed in days of the year and the ordinates in mm. The dates of the onset and end of the rainy season are symbolized by the grey vertical lines for the average regime of the region, orange for the seasonal type.

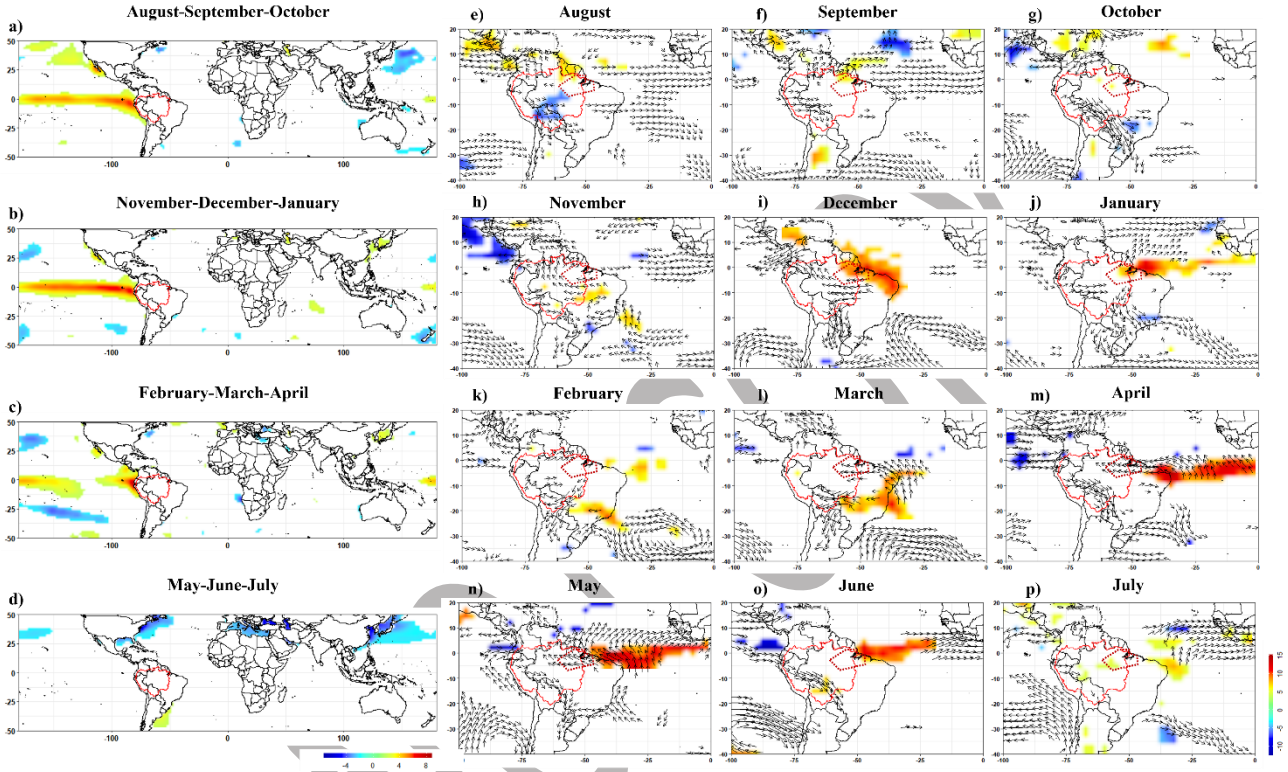

Figure 5 For seasonal type 1 of the North-East Region (Figure 4a1), seasonal composite maps of significant anomalies from August year-1 to July year-0 of SST (in °C; from a to d) in the left panels, and monthly composite maps of significant anomalies from August year-1 to July year-0 of OLR (W/m²) and IWV (vectors, in kg m-1 day-1) for South America (from e to p) in the right panels. Significant anomalies are greater than 2 σ. Anomalies are calculated with respect to the period 1981-2013. The red solid line represents the Amazon watershed and the red dotted line represents the North-East region.

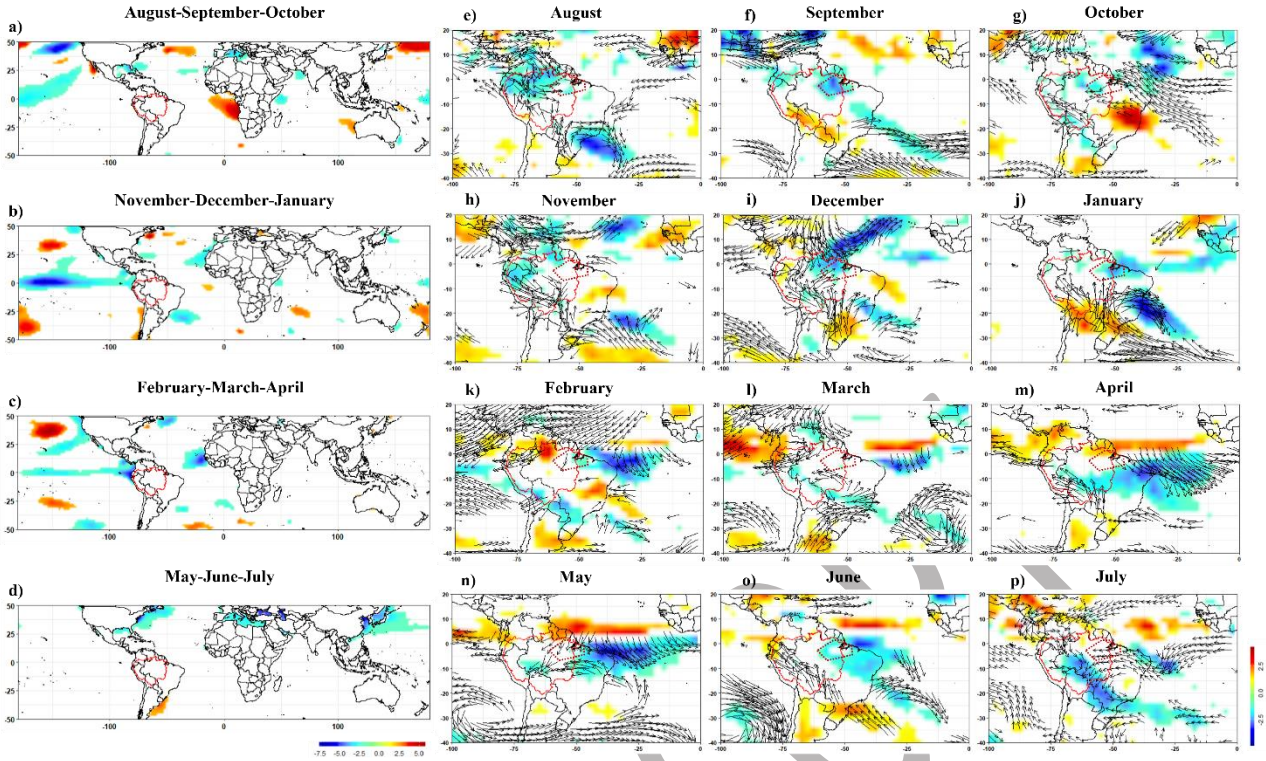

836

837 *Figure 6 Same legend as for Figure 5, but for type 3 (Figure 4a3) in the North-East Region.*

838

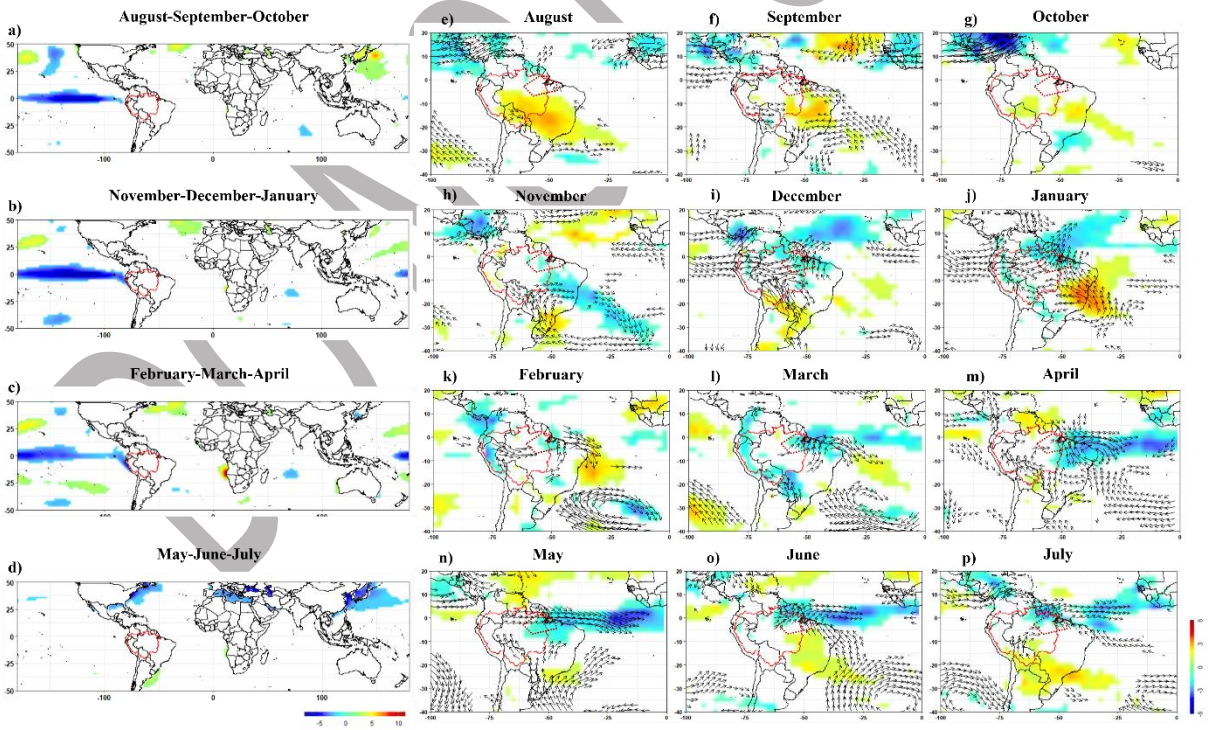

839

840 *Figure 7 Same legend as for Figure 5, but for type 4 (Figure 4a4) in the North-East Region.*

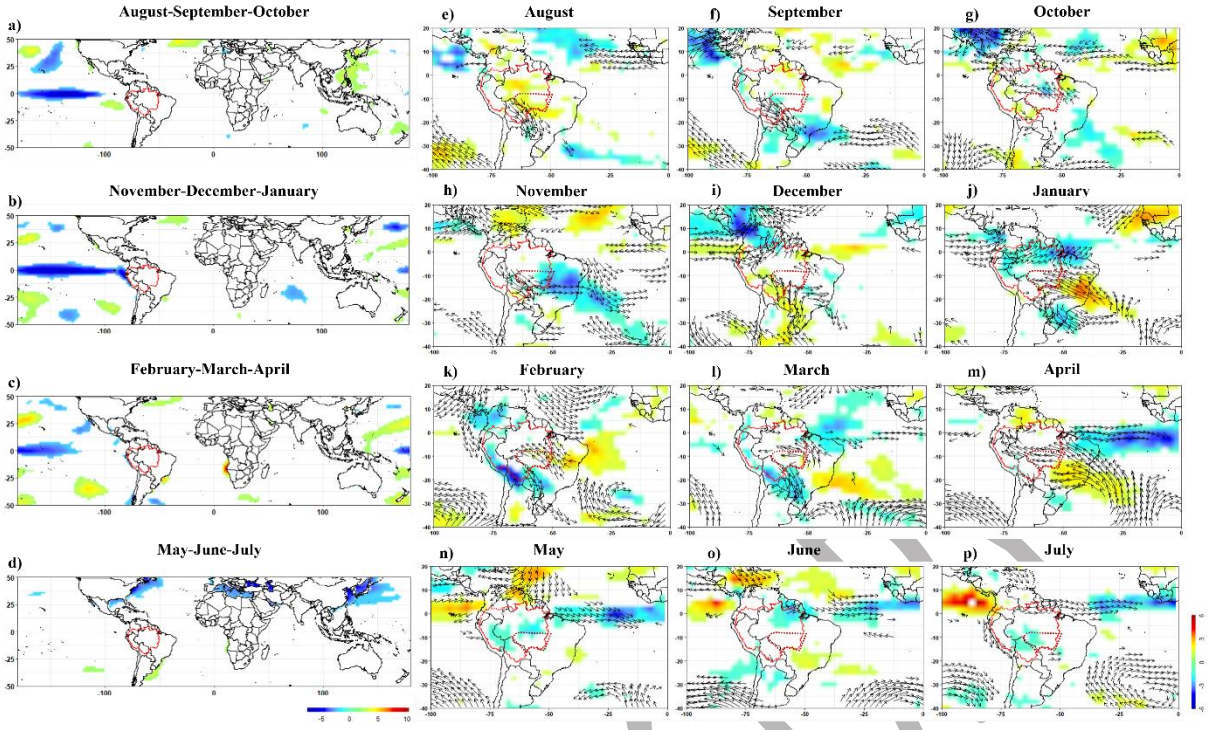

Figure 8 Same legend as for Figure 5, but for type 3 (Figure 4b3) in the South-East Region except for the red dotted line that represents the South-East region.

Table 1 Characteristics of seasonal type in the Amazon basin.

Rainy season dates \ Rainfall anomaly		Excess all season	Deficit all season	Alternating anomalies
No rainy season dates		Andes type 2	Andes type 1	Andes type 3
Equal duration	normal onset + normal demise			South-East type 1 North-East type 2
Shifted season	early onset + early demise			South-East type 2 Rio Negro type 2
Shorter season	normal onset + early demise			South-East type 3
	late onset + normal demise			North type 2 Rio Negro type 1 Rio Negro type 3 South-East type 4
	late onset + early demise		Nord-East type 1 South type 2	
Longer season	normal onset + late demise	North type 4		North-East type 3
	early onset + normal demise	South type 1 Rio Negro type 4	South type 3	North type 3
	early onset + late demise	North-East type 4		North type 1 South type 4 Andes type 4

Tableau 2 Synthesis of Pacific and Atlantic oceanic phases associated with Northeast Region seasonal types. The Central or Eastern type of ENSO events is based on the classifications proposed by Andreoli et al. (2016), Tedeschi et al. (2016) and Pillai et al. (2020). Event intensity is based on the CPC-NCEP NOAA Oceanic Niño Index (ONI): weak anomaly [0.5; 0.9]; moderate anomaly [1; 1.4]; strong anomaly [1.5; 1.9]; very strong anomaly ≥ 2. The Atlantic phases are based on the index

provided by the NOAA/ESRL Physical Science Division and CIRES CU, Boulder, Colorado, from their website at https://psl.noaa.gov/. The phase is considered positive or negative for an anomaly beyond 0.1°C. EN = El Niño; LN = La Niña.

Seasonnal Types	Year	Pacific SST Phase	NTATL SST phase	STATL SST phase
1 : very dry and shorter rainy season	1992-93	Neutral	Negative	Negative
	1996-97	Neutral	Neutral	Negative
	1997-98	Very strong East EN	Positive	Positive
	2002-03	Moderate Central EN	Neutral	Positive
	2004-05	Weak Central EN	Positive	Positive
	2006-07	Weak East EN	Positive	Positive
	2011-12	Weak central LN	Neutral	Neutral
3 : contrasted anomalies and longer rainy season	1984-85	Weak East LN	Negative	Positive
	2008-09	Weak central LN	Neutral	Positive
4 : humid and longer rainy season	1983-84	Weak central LN	Negative	Positive
	1994-95	Moderate Central EN	Neutral	Positive
	1995-96	Weak East LN	Positive	Positive
	1998-99	Strong Central LN	Neutral	Positive
	1999-00	Strong Central LN	Negative	Positive
	2005-06	Weak LN	Positive	Positive
	2007-08	Strong LN	Neutral	Positive

Tableau 3 Synthesis of Pacific and Atlantic oceanic phases associated with South-East Region seasonal type. The Central or Eastern type of ENSO events is based on the classifications proposed by Andreoli et al. (2016), Tedeschi et al. (2016) and Pillai et al. (2020). Event intensity is based on the CPC-NCEP NOAA Oceanic Niño Index (ONI): weak anomaly [0.5; 0.9]; moderate anomaly [1; 1.4]; strong anomaly [1.5; 1.9]; very strong anomaly ≥ 2. The Atlantic phases are based on the index provided by the NOAA/ESRL Physical Science Division and CIRES CU, Boulder, Colorado, from their website at https://psl.noaa.gov/. The phase is considered positive or negative for an anomaly beyond 0.1°C.

Seasonal Type	Year	Pacific SST Phase	NATL SST phase	SATL SST phase
3: contrasted anomalies and shorter rainy season	1983-84	Weak central LN	Negative	Negative
	1995-96	Weak East LN	Positive	Positive
	1998-99	Strong Central LN	Neutral	Positive
	2000-01	Weak LN	Negative	Negative
	2001-02	Neutral	Positive	Positive